PROCEEDINGS OF SCIENCE

On the synchrotron origin of MeV-GeV emission of Crab Nebula: Constraints from LHAASO's Observation

Cui-Yuan Dai,[a,b,*] **Ming-Yu Lei,**[c] **Xiao-Yuan Huang,**[c] **Ruo-Yu Liu**[a,b] **and Xiang-Yu Wang**[a,b]

[a] *School of Astronomy and Space Science, Nanjing University, Nanjing 210093, China*

[b] *Key Laboratory of Modern Astronomy and Astrophysics (Nanjing University), Ministry of Education, Nanjing 210093, China*

[c] *Key Laboratory of Dark Matter and Space Astronomy, Purple Mountain Observatory, Chinese Academy of Sciences, Nanjing 210033, China*

E-mail: ryliu@nju.edu.cn, xywang@nju.edu.cn

Crab Nebula is the standard candle for high-energy gamma-ray astronomy showing a stable emission over a long period of time. At relatively lower energy, i.e., in the MeV-GeV gamma-ray band, however, the nebule presents flares from time to time, lasting over a wide range of durations from hours up to months. While the MeV-GeV emission of Crab Nebula is believed to arise from the synchrotron radiation of relativistic electrons/positrons, the cutoff frequency of the spectrum during flares sometimes extends beyond the so-called synchrotron burn-off limit. Some previous studies explained the flares as the Doppler-boosted synchrotron emission from newly ejected blobs which move relativistically toward observers. We aim to test this model by comparing the expected inverse Compton (IC) radiation from the blob, which is supposed to appear in the ultrahigh-energy gamma-ray band, with the measurement of LHAASO. By doing so, we may impose constraints on some key parameters of the model. Based on the obtained constraints, we discuss the origin of the MeV-GeV emission of Crab Nebula.

38th International Cosmic Ray Conference (ICRC2023)
26 July - 3 August, 2023
Nagoya, Japan

*Speaker

PoS(ICRC2023)875

1. Introduction

The Crab Nebula, generated from the supernova explosion and observed in 1054 CE, is one of the brightest gamma-ray nebula powered by the rotational energy of the Crab pulsar. As its radiation is consistently stable, it has been widely used as a reference to calibrate detectors and instruments in the mentioned energy ranges. However, the enhancement of radiation has been found in the MeV-GeV band, which has been considered to be generated by the synchrotron emission of electrons/positrons (we do not distinguish positrons from electrons in the following discussion for simplicity) and called "flare". These flares can last from hours up to months, during which the cutoff frequency of the spectrum may exceed the synchrotron burn-off limit. In addition, LHAASO detected the PeV photons from Crab Nebula [1]. A possible origin of these flares in the MeV-GeV band can be the emission from blobs moving relativistically towards observer [2, 3]. However, the discussion in previous work did not use the LHAASO data, since LHAASO only detects the γ-ray signals from the Crab Nebula after December 2019 [4]. In this paper, we combine Fermi-LAT and LHAASO observations to discuss the properties of blob emission, the possible value of the acceleration ratio of electrons, and the origin of flares and PeV photons. We first show the Fermi-LAT data analysis in Sec.2, and then discuss the possible parameters in the frame of the blob emission model in Sec.3 and Sec.4. Lastly, we give a brief discussion in Sec.5.

2. Fermi-LAT Data Analysis

2.1 Phase folding

Since the central pulsar of Crab Nebula emits strong radiation in the γ-ray band, we need to eliminate the contribution of the central pulsar. According to [5], we utilized the pulsar analysis package TEMPO2 and the monthly ephemeris of the Crab pulsar [6] to assign phases to γ-ray photons during MJD 58065-58975, which includes the time window of LHAASO detection. However, as the ephemeris lacks data between MJD 58925-58975, we divided the data into two parts: MJD 58065-58925 and 58975-59979. The selected events are classified as the P8R3 SOURCE event category, with energies ranging from 80 MeV to 300 GeV and angles within 25 degrees of the Crab pulsar. The light curve, folded according to the pulsar phase, is shown in Fig.1, from which we choose phase 0.44-0.84 and 0.15-0.55 to eliminate the pulsar emission for MJD 58065-58925 and 58975-59979, respectively.

2.2 Searching the flares from the light curve of Crab Nebula

To conduct data analysis, we first select γ-ray photons that pass the P8R3 SOURCE event class selection, with energies from 100 MeV to 300 GeV and angular deviations within 15 degrees from the Crab pulsar. We then analyze the data using an unbinned maximum likelihood fit with the module pyLikelihood in the Fermitools for each time interval. Additionally, we use the module SummedLikelihood to perform a joint likelihood analysis of the two time intervals.

After conducting the joint likelihood analysis, we divided the data into 4 days/bin. Each time bin involved several free parameters in the likelihood fit, including the normalizations and spectral indices of both nebula components and the normalizations of the Galactic and isotropic diffuse backgrounds. All other parameters were kept fixed at their best-fit values from the joint likelihood

analysis. We selected time bins with fluxes 5σ higher than the average flux according to [5] to identify flares. The light curve of the two intervals is shown in Fig.2, where the red data represents the flare state as defined above, and the horizontal line represents the average flux of the Crab Nebula.

2.3 Spectrum and time window of the flare

We created a light curve with a bin width of 1 day and used the Bayesian block method [7] to determine the time windows of flares, one of which is shown in Fig.3. Subsequently, we calculated the spectral energy distributions (SED) of the flares' low-energy component by dividing the data into 9 logarithmically evenly distributed energy bins from 100 MeV to 5 GeV. The normalizations of the low-energy component are the only parameters set free during the SED fits while other parameters are fixed to the values obtained in the previous section for the joint likelihood analysis of all time intervals. If the significance is lower than 2σ in particular energy bins, the 95% upper limits are derived, as depicted in Fig.4.

As mentioned above, LHAASO only detects the γ-ray signals from the Crab nebula after December 2019 [4] and the flares after December 2019 has similar properties (spectrum in MeV-GeV band, duration, and so on), we use the flare whose time window is 58065 – 58925 to discuss the properties of blob emission in following sections.

3. The origin of MeV-GeV emission of Crab Nebula

As mentioned above, relativistic blobs can explain the flare emission in the MeV-GeV band. We first calculate the electron distribution and then fit the multi-band observation of the average flux of the Crab Nebula. Lastly, we add the contribution of blob emission and constraint the acceleration efficiency of the relativistic blob by fitting the Fermi-LAT observation in the MeV-GeV band and limiting the TeV emission by LHAASO sensitivity curve during the flare.

3.1 Theoretical model

3.1.1 Electron distribution

We consider two types of electrons, i.e., type I: which is injected continuously with a power-low spectrum, contributing to the average flux of emission from the Crab Nebula, and type II: which is injected as a "blob" with a spectrum following Maxwellian distribution, contributing to the flare emission.

The injected differential spectra of type I $Q_{e,\mathrm{I}}$ and type II $Q_{e,\mathrm{II}}$ electron can be written as:

$$Q_{e,\mathrm{I}}(\gamma_e, t) = Q_{0,\mathrm{I}}(t) \begin{cases} (\gamma_e/\gamma_{\max})^{\alpha_\mathrm{l}}, & \gamma_e < \gamma_{\max}, \\ (\gamma_e/\gamma_{\max})^{\alpha_\mathrm{h}}, & \gamma_e > \gamma_{\max}, \end{cases} \tag{1}$$

and

$$Q_{e,\mathrm{II}}(\gamma_e) = Q_{0,\mathrm{II}}\gamma_e^2 \exp(\gamma_e/\gamma_\mathrm{c}). \tag{2}$$

For electron type I, we follow the method in [8] to calculate the electron distribution. The differential density in the spherical system can be written as:

$$\frac{\partial n_e}{\partial t} = D_e \frac{\partial^2 n_e}{\partial r^2} + \left[\frac{1}{r^2}\frac{\partial}{\partial r}(r^2 D_e) - V\right]\frac{\partial n_e}{\partial r} - \frac{1}{r^2}\frac{\partial}{\partial r}[r^2 V] n_e + \frac{\partial}{\partial \gamma_e}[\dot{\gamma}_e n_e] + Q_e, \tag{3}$$

where $V = V(r)$ is the bulk velocity, $D_e \equiv D_e(r, \gamma_e, t)$ is the diffusion coefficient of particles, $\dot{\gamma}_e$ is the summation of particle energy losses, and Q_e is the source term.

3.1.2 Radiation from electrons

We calculate the differential spectrum of synchrotron and IC scattering according to [9]:

$$\begin{aligned} Q_\gamma^{\rm syn}(r, \epsilon, t) &= \int_0^\infty n_e(r, \gamma, t) P_{\rm syn}(r, \epsilon, \gamma, t) d\gamma, \\ Q_\gamma^{\rm ics}(r,\ \epsilon, t) &= \int_0^\infty n_e(r,\ \gamma, t) P_{\rm IC}(r,\ \epsilon,\ \gamma, t) d\gamma. \end{aligned} \tag{4}$$

The emissivity $P_{\rm syn}(r, \epsilon, \gamma, t)$ and $P_{\rm IC}(r,\ \epsilon,\ \gamma, t)$ can be written as:

$$\begin{aligned} P_{\rm syn}(r, \epsilon, \gamma, t) &= \frac{\sqrt{3} e^3 B(r, t)}{h \epsilon m_{\rm e} c^2} F\left(\frac{\epsilon}{\epsilon_{\rm c}}\right), \\ P_{\rm IC}(r, \epsilon, \gamma, t) &= \frac{3}{4}\frac{\sigma_{\rm T} c}{\gamma^2} \int_0^\infty \frac{n_{\rm sph,\ j}(r, \epsilon_i, t)}{\epsilon_i} f(q, \Gamma) d\epsilon_i. \end{aligned} \tag{5}$$

The observed intensity $I_\nu(\nu)$ ($\rm erg\,cm^{-2}\,s^{-1}\,Hz^{-1}\,sr^{-1}$) will be boosted if the blob moving relativistically toward the observer. The relation between intensity $I'_{\nu'}(\nu')$ in the observed frame and that $I_\nu(\nu)$ in the comoving frame is:

$$I_\nu(\nu) = \delta^3 I'_{\nu'}(\nu'), \tag{6}$$

where δ is the Doppler factor and $\nu = \delta \nu'$.

We note that the number density and energy of the target photons field will both be boosted by δ, so the observed intensity generated from the IC process in the blob should be boosted by another factor δ^2. Then we have:

$$\begin{aligned} I_{\nu,{\rm syn}}(\nu) &= \delta^3 I'_{\nu',{\rm syn}}(\nu'), \\ I_{\nu,{\rm IC}}(\nu) &= \delta^5 I'_{\nu',{\rm IC}}(\nu'). \end{aligned} \tag{7}$$

3.1.3 Constraint on the acceleration efficiency of relativistic blob

The observed flux from single blob $F_{\nu,{\rm bolb}}$ depends on four parameters: total energy $E_{\rm blob}$ of electrons in the blob, the magnetic field $B_{\rm blob}$ in the blob, cutoff energy $E_{\rm c} = \gamma_{\rm c} m_e c^2$ and Doppler factor δ, i.e., $F_{\nu,{\rm bolb}} = F_{\nu,{\rm bolb}}(E_{\rm blob}, B_{\rm blob}, E_{\rm c}, \eta, \delta)$. $E_{\rm c}$ is dependent on magnetic field B and acceleration efficiency η: electrons can be accelerated to maximum energy (cutoff energy) when the cooling timescale $t_{\rm cooling} \simeq t_{\rm syn} = 3 m_e c/(4\sigma_T \gamma_e U_B)$ is equal to the acceleration timescale $t_{\rm a} = 2\pi\gamma_e c/(\eta e B)$ (the energy dissipation during IC process can be ignored since the electrons

dissipate energy mainly through synchrotron process in a strong magnetic field, which is $107\,\mu G$ by fitting to the average flux of Crab Nebula, see Fig.4), so the maximum energy of electrons is $E_{\rm c} = m_e c^2\sqrt{6\pi\eta/(\sigma_T B)}$. Therefore the observed flux from a single blob can be written as $F_{\nu,\rm bolb} = F_{\nu,\rm bolb}(E_{\rm blob}, B_{\rm blob}, \eta, \delta)$. We consider two cases of magnetic field: In case I, the magnetic field in the blob is compared with that in the Crab Nebula ($B_{\rm blob} = 107\,\mu G$). In case II, the blob is injected with the strong magnetic field ($B_{\rm blob} = 1$ mG). Acceleration efficiency η is a free parameter. $E_{\rm blob}$ and δ are degenerate with η, both of which can be determined by η and the observation in the MeV-GeV band during the time window of the flare.

Fig.5 shows the emission from both the electron from type I (the black solid line) and type II (blob emission, the dashed lines), from which we can see a low acceleration efficiency will lead to a larger ratio of $R_\nu = I_{\nu,\rm IC}/I_{\nu,\rm syn}$: as mentioned above, δ is degenerate with η, lower acceleration efficiency needs larger δ to fit the observation in MeV-GeV band. According to Eq.7, the Doppler boosting of IC emission is stronger than that in the synchrotron process: $I_{\nu,\rm IC}/I_{\nu\rm syn} = \delta^2(I'_{\nu',\rm IC}/I'\nu', \rm syn)$, so large δ, which is resulted from low η, will lead to larger R_ν.

However, the TeV flux from the source cannot exceed the sensitivity curve of LHAASO because the timing of LHAASO's detection of PeV photons is not consistent with the flares in the MeV-GeV band (see Fig.2 and table S1 in [1]), implying that the η has the lower limit, which can be seen from Fig.4: $\eta_{\rm min}$ is 4×10^{-2} and 9.0×10^{-3} for $B = 107\,\mu$G and 1 mG, respectively.

On the other hand, η also has an upper limit, above which the frequency of peak flux is larger than that from the observation even though there is no Doppler boosting ($\delta = 1$). As shown in Fig.4, $\eta_{\rm max}$ is $\simeq 0.114$ for both $B = 107\,\mu$G and 1 mG.

4. The origin of TeV emission of Crab Nebula

According to Sec.2.2, the incidence rate of flares is about $1 \sim 2$ events/year, which is consistent with [5]. As mentioned above, the timing of LHAASO's detection of PeV photons does not align with the flares in the MeV-GeV band, therefore we can get the upper limit of TeV flux, which is about $10^{-3}\,\rm erg\,cm^{-2}\,s^{-1}$ (see Fig.4). From Sec.2.3, we know that single flare only last for days, so the year-average TeV flux generated by blobs is less than $10^{-4}\,\rm erg\,cm^{-2}\,s^{-1}$, which can not explain the origin of PeV photons detected by LHAASO [1].

We argue that many "small" blobs can be continuously, stably injected from the termination shock, and these blobs can explain the emission in the MeV and PeV bands of the Crab Nebula.

We fix the magnetic field $B_{\rm blob}$ of blobs to $107\,\mu$G and $1000\,\mu$G, and assume δ and η are following Gaussian distribution, whose mean value and variance are δ_0 and η_0, respectively. The distribution of the electron energy in blobs satisfies the self-organized criticality (SOC) system, in which the probability density function $f(E_{\rm blob}) = N_{\rm blob}E_{\rm blob}^{-1.5}$ with Euclidean space dimensions $S = 3$ [10], where $N_{\rm blob}$ is the normalization determined by observation. Then the average flux of blobs can be written as:

$$\bar{F}_{\nu,\rm bolb} = \int\int\int f_\eta(\eta) f_\delta(\delta) f_{E_{\rm blob}}(E_{\rm blob}) F_{\nu,\rm bolb}(E_{\rm blob}, B_{\rm blob}, \eta, \delta)\, d\eta d\delta dE_{\rm blob}. \quad (8)$$

The spectrum of "small" blobs is shown in Fig.5. The average acceleration $\eta_0 = 2\times10^{-2}$ and 5×10^{-3} for $B_{\rm blob} = 107\,\mu$G and 1 mG, respectively.

5. Discussion

We use the blob emission model to explain the enhancement emission in the Mev-GeV band and the origin of PeV photons detected by LHAASO [1] from the Crab Nebula. By fitting to the data, we get the following conclusions:

(1) The emission from blobs can explain the flares in the MeV-GeV band. However, the time of detecting the flares is inconsistent with the PeV photons, therefore we can constrain the acceleration ratio of the blobs from the upper limits in the TeV band given by LHAASO sensitivity curve: $\eta_{\rm min}$ is 4×10^{-2} and 9.0×10^{-3} for $B_{\rm bolb} = 107\,\mu$G and 1 mG, respectively.

(2) The emission of blobs generated during the flares' state can not explain the PeV photons detected by LHAASO [1]. We argue that the origin of the PeV photons should be the "small flares", which have smaller radiation energy and happen more frequently. By fitting the observed spectrum of Crab Nebula in MeV-GeV and PeV band, we find the average acceleration ratio in blobs is: $\eta_0 = 2 \times 10^{-2}$ and 5×10^{-3} for $B_{\rm blob} = 107\,\mu$G and 1 mG, respectively.

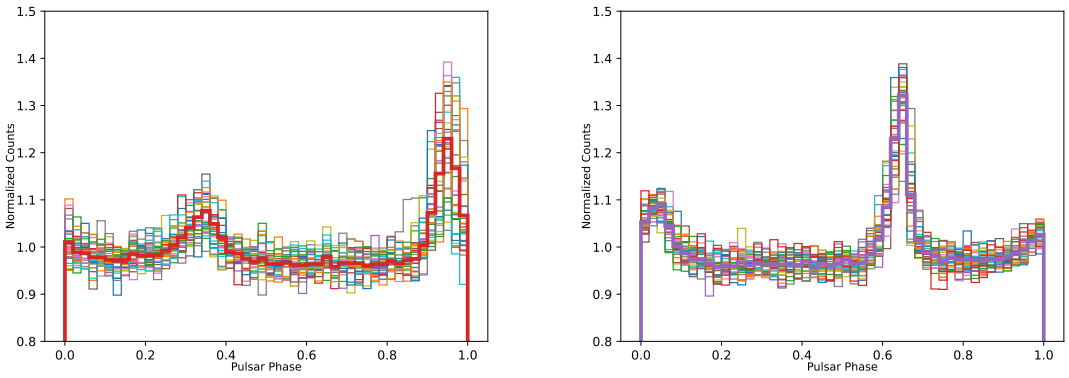

Figure 1: Phase folding in two periods. Left panel: MJD 58065-58925; right panel: MJD 58975-59979.

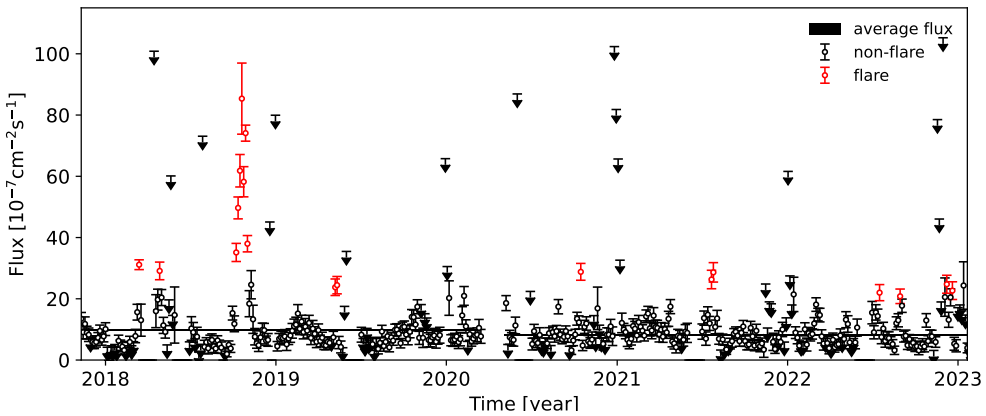

Figure 2: The light curve (4 days per bin) of the two periods (MJD 58065-58925 and 58975-59979).

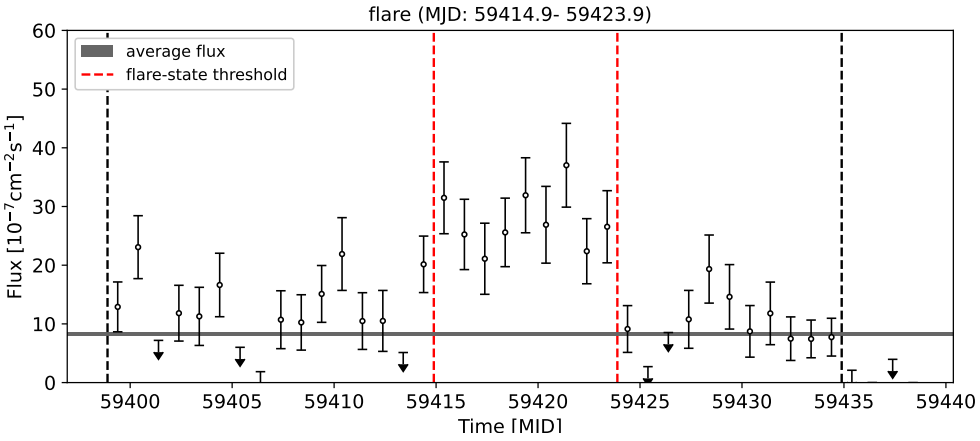

Figure 3: The Light curve of single flare (1 day per bin). The time window of the flare is separated by red dashed lines.

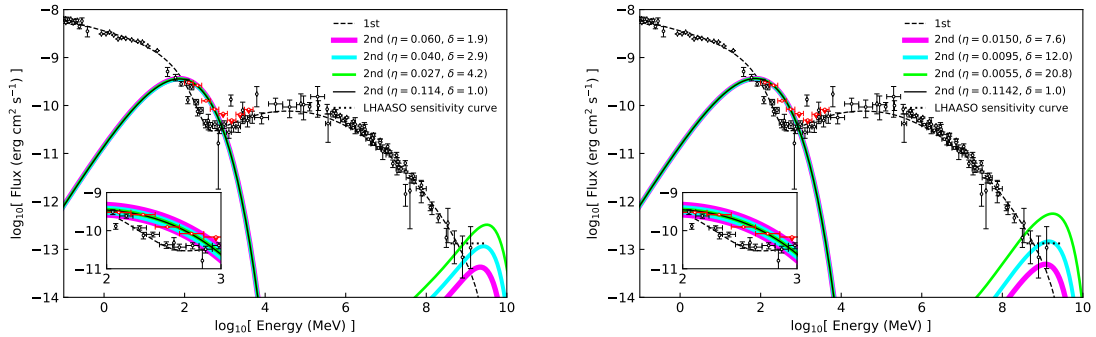

Figure 4: The expected spectrum of the Crab Nebula. The dashed line is the emission from electrons type I, and the solid line is the emission from electrons type II. The black data is the average flux, and the rad data is the flux during the time window of the flare. Left panel: $B_{\rm blob} = 107\,\mu$G; right panel: $B_{\rm blob} = 1$ mG.

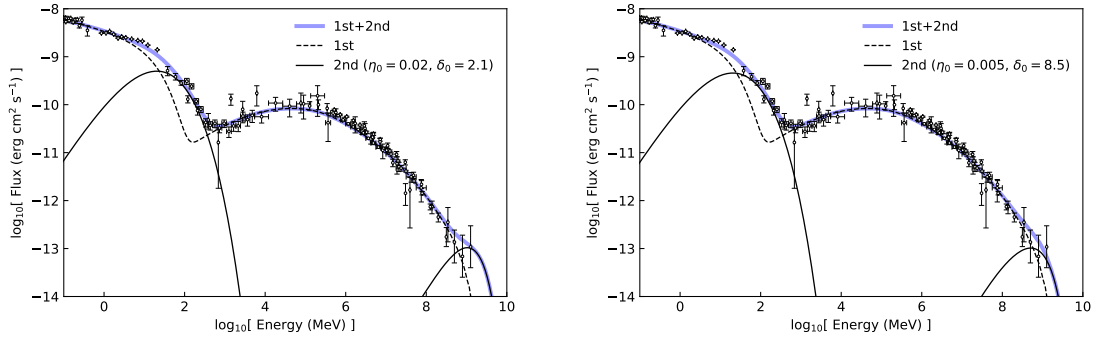

Figure 5: Same as Fig.4, but the cutoff energy of electrons type I is set to 2 PeV.

References

[1] Lhaaso Collaboration, Cao Z., Aharonian F., An Q., Axikegu, Bai L. X., Bai Y. X., et al., 2021, Sci, 373, 425. doi:10.1126/science.abg5137

[2] Kohri K., Ohira Y., Ioka K., 2012, MNRAS, 424, 2249. doi:10.1111/j.1365-2966.2012.21388.x

[3] Lyutikov M., Balsara D., Matthews C., 2012, MNRAS, 422, 3118. doi:10.1111/j.1365-2966.2012.20831.x

[4] Aharonian F., An Q., Axikegu, Bai L. X., Bai Y. X., Bao Y. W., Bastieri D., et al., 2021, ChPhC, 45, 025002. doi:10.1088/1674-1137/abd01b

[5] Huang X., Yuan Q., Fan Y.-Z., 2021, ApJ, 908, 65. doi:10.3847/1538-4357/abd2b7

[6] Lyne A. G., Pritchard R. S., Graham Smith F., 1993, MNRAS, 265, 1003. doi:10.1093/mnras/265.4.1003

[7] Scargle J. D., Norris J. P., Jackson B., Chiang J., 2013, ApJ, 764, 167. doi:10.1088/0004-637X/764/2/167

[8] Peng Q.-Y., Bao B.-W., Lu F.-W., Zhang L., 2022, ApJ, 926, 7. doi:10.3847/1538-4357/ac4161

[9] Blumenthal G. R., Gould R. J., 1970, RvMP, 42, 237. doi:10.1103/RevModPhys.42.237

[10] Aschwanden M. J., 2012, A&A, 539, A2. doi:10.1051/0004-6361/201118237